Enhanced Performance of Streamline-Traced External-Compression Supersonic Inlets

John W. Slater[*]

NASA John H. Glenn Research Center at Lewis Field, Brook Park, Ohio 44135 USA

Abstract

A computational design study was conducted to enhance the aerodynamic performance of streamline-traced, external-compression inlets for Mach 1.6. Compared to traditional external-compression, two-dimensional and axisymmetric inlets, streamline-traced inlets promise reduced cowl wave drag and sonic boom, but at the expense of reduced total pressure recovery and increased total pressure distortion. The current study explored a new parent flowfield for the streamline tracing and several variations of inlet design factors, including the axial displacement and angle of the subsonic cowl lip, the vertical placement of the engine axis, and the use of porous bleed in the subsonic diffuser. The performance was enhanced over that of an earlier streamline-traced inlet such as to increase the total pressure recovery and reduce total pressure distortion.

Nomenclature

b_{stcl}	thickness of the subsonic cowl lip
β_{stex}	angle of the terminal shock
C_{Dwave}	cowl wave drag coefficient
D	diameter
$DIST$	simple distortion descriptor
Δx_{stcl}	displacement of the subsonic cowl lip
Δs^{*}_{ref}	reference grid spacing
Δs_{sym}	grid spacing at the symmetry boundary
Δs_{thrt}	grid spacing at the throat
IDC	circumferential distortion descriptor
IDR	radial tip distortion descriptor
p_t	total pressure
L_{exd}	length of the external supersonic diffuser
M	Mach number
θ_{stcl}	angle of the subsonic cowl lip
θ_{stle}	angle of the cowl lip leading edge
x,y	Cartesian coordinates
y_{inlet}	y-coordinate of the inlet axis
y_{stex}	y-coordinate of the tracing curves axis
W	flow rate

Subscripts

0	freestream conditions
2	engine-face conditions
C	corrected engine-face conditions
EX	conditions ahead of the terminal shock
cap	design inlet capture
$stex$	conditions at the Busemann outflow

Introduction

A streamline-traced inlet has an external supersonic diffuser that is formed from the collection of streamlines through a compressive, supersonic parent flowfield. A methodology for the design of streamline-traced inlets for commercial supersonic flight at Mach 1.6 was presented in Ref. 1. This methodology was based on streamline tracing through a parent flowfield consisting of the axisymmetric Busemann flowfield. An oblique leading edge shock and a normal, terminal shock were then imposed onto the streamline-traced flowfield. The performance of the resulting inlets were compared to traditional two-dimensional ramp and axisymmetric spike inlets. The streamline-traced inlets had a fraction of the wave drag of the traditional inlets with a slightly lower total pressure recovery. Further, the streamline-traced inlets produced lower external sound pressures, which relate to sonic boom disturbances. However, the streamline-traced inlets possessed higher levels of total pressure distortion at the engine face.

The methodology of Ref. 1 involved several aerodynamic and geometric procedures that did not have a solid physical basis and contained some confusing design factors. Reference 2 discussed a new methodology with a parent flowfield that contained a leading-edge oblique shock and a strong, oblique terminal shock with subsonic outflow.[2] The current paper discusses the application of this new methodology to the Mach 1.6 inlet design problem of Ref. 1 to enhance the aerodynamic performance of a streamline-traced, external-compression inlet. The next section provides a summary of the new streamline-traced methodology as discussed in Ref. 2. The methodology was implemented into the SUPIN supersonic inlet design and analysis tool.[3] SUPIN was used to size inlets and generate surfaces and grids for analysis using CFD methods. The Wind-US CFD code was used to compute the steady, turbulent flow through the inlets and compute the inlet aerodynamic performance in terms of the flow rates, total pressure recovery, cowl wave drag, and total pressure distortion.[4] The results present the effects of the design factors and the approaches toward a "best" inlet configuration with enhanced performance at Mach 1.6.

Inlet Design Methodology

The streamline-tracing methodology of Ref. 2 was used to design inlets for Mach 1.6. The methodology

[*] Research Aerospace Engineer, Inlet and Nozzle Branch.

used an axisymmetric parent flowfield that contained a conical shock and internal conical flowfield at the leading edge that was mated with an axisymmetric Busemann flowfield. The Busemann flowfield had an outflow with a strong conical shock that resulted in subsonic outflow, which was desirable for an external-compression inlet. The numeric solution of the parent flowfield required specification of the supersonic inflow Mach number (M_0), the angle of the deflection of the leading edge (θ_{stle}), and the subsonic outflow Mach number (M_{stex}). Figure 1 shows a schematic of the parent flowfield and the streamline tracing.

The leading edge flowfield was the internal conical flowfield type A (ICFA) of Mölder.[5] The final downstream ray of the ICFA flowfield solution is shown in Fig. 1 as the dashed line for the first ray downstream of the leading edge shock.

Figure 1. Parent flowfield.

The Busemann flowfield was computed in the upstream direction starting with the uniform, subsonic outflow of the strong conical, terminal shock. The solution of the Busemann flowfield involved an iterative procedure to match up conditions at the upstream ray with the downstream ray of the ICFA flowfield. The angle of the strong shock (β_{stex}) was varied within the iteration. Reference 2 discussed the details of the procedure to match the ICFA and Busemann flowfields.

The streamline tracing started at tracing curves placed within the uniform outflow of the Busemann flowfield. Figure 1 shows two tracing curves – one on the top and one on the bottom. The curves were defined by super-ellipses. Super-ellipses allow a family of shapes including circles, ellipses, and curves approximating rectangles. In this case, the tracing curves formed a circle. The tracing curves were placed in the flowfield at a specified offset (y_{stex}) from the axis of the solution. Points were distributed about the circumference of the tracing curves and the surface of the supersonic diffuser was formed by tracing streamlines in the upstream direction with each streamline starting at the points on the tracing curves.

A variety of inlet shapes can be obtained by selection of the shape and placement of the tracing curves. A non-zero off-set resulted in the scarfing of the leading edge, which was advantageous for providing relief of excess

inlet flow downstream of the terminal shock. The offset placed the tracing curves above the solution axis with the bottom tracing curve slightly above the axis. This resulted in the shortest supersonic diffuser.

Figure 2 shows a streamline-traced inlet created with circular tracing curves offset from the axis. The inlet axis corresponds to the axis of the tracing curves. The leading edge is scarfed and the "nose" is the forward point on the leading edge. The red lines are the approximate locations of the leading edge and terminal shocks.

Figure 2. Streamline-traced inlet.

Most of the leading edge will encounter supersonic flow; however, the portion of the leading edge downstream of the terminal shock will encounter subsonic flow. This portion is called the subsonic cowl lip. Figure 2 shows the approximate extent of the supersonic leading edge and the subsonic cowl lip for the example inlet. The leading edge of the inlet is made slightly blunt through the use of an elliptical profile for the leading edge. The thickness of the elliptical profile is made very small for the supersonic flow to minimize entropy gradients about the blunt-lip shock. The thickness of the subsonic cowl lip can be made thicker to be more favorable to the local subsonic flow. The design factor for the thickness of the subsonic cowl lip is the thickness at the inlet symmetry plane (b_{stcl}). The local angle of the subsonic cowl lip can be made different from the angle of the supersonic leading edge to align the subsonic cowl lip with the subsonic flow. The design factor for the subsonic cowl lip angle is the angle of the subsonic cowl lip at the inlet symmetry plane (θ_{stcl}). The thickness and angle about the circumferential extent of the subsonic cowl lip is established through a smooth transition of the thickness and angle between the symmetry plane and the start of the supersonic leading edge.

Additional spillage beyond that provided by the scarfing of the leading edge can be affected by displacing

the subsonic cowl lip further downstream. The design factor for this is the axial displacement of the subsonic cowl lip at the inlet plane of symmetry (Δx_{stcl}). Figure 3 shows the combined effect of axial displacement and cowl lip angle. The change in cowl lip angle affects the cowl exterior shape below the subsonic cowl lip.
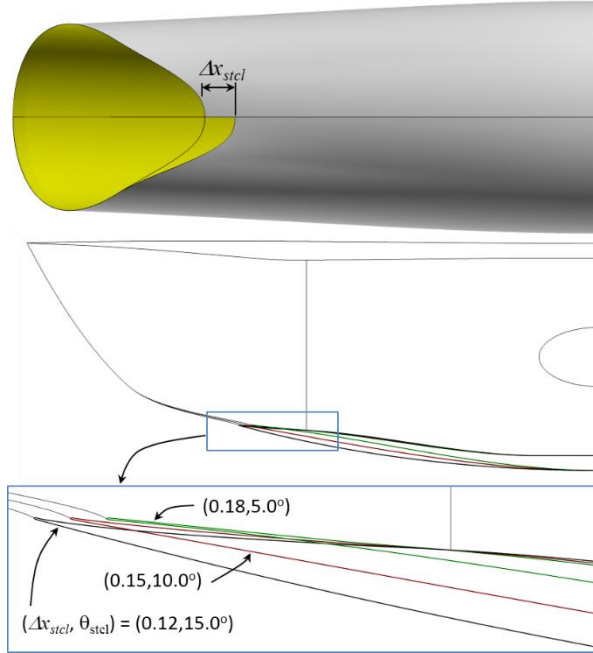

Figure 3. Subsonic cowl lip design factors.

The parent flowfield is an inviscid solution. To account for boundary layer growth, the streamline-traced surface of the supersonic diffuser is adjusted radially outward a distance approximate to the displacement thickness of the boundary layer. The amount of adjustment along the diffuser is linearly varied from the leading edge to the end of the supersonic diffuser.

The end of the supersonic diffuser is called the "shoulder" of the inlet and has a slope computed by the Busemann flowfield solution. Downstream of the shoulder, the flow is turned toward the axial direction. This sharp change in surface angle is replaced with a circular arc to assist the turning of the flow. The input factor for this adjustment is the axial extent of the circular arc.

Downstream of the shoulder and subsonic cowl lip, the flow is assumed to be subsonic at critical inlet operation. The subsonic diffuser is created by a smooth transition of the shape of the tracing curve to the circular shape of the engine face. The engine face is defined by the specified diameter (D_2) and spinner hub-to-tip ratio. The profile of the spinner is specified to be elliptical with an aspect ratio of two. The vertical placement of the engine face (y_2) is a design factor. The placement of the engine face affects how much the flow has to turn over the surfaces of the subsonic diffuser.

SUPIN Inlet Design Tool

The streamline-tracing methodology described in the previous section was implemented into the SUPIN supersonic inlet design and analysis tool.[3] SUPIN uses analytical and numerical methods to design and analyze inlets and generate inlet geometry using a small set of design factors. The parent flowfield of the previous section was computed through a solution of the Taylor-Maccoll equations and compressible flow relations.[6] The streamlines through the parent flowfield were determined through numerical integration in the upstream direction starting at points on the tracing curves. Planar geometry modeling methods were used to construct the surfaces of the inlets.

The performance of the inlet was calculated using compressible flow relations, empirical models, and computational solutions. The cowl wave drag was computed using a small disturbance analysis over an axisymmetric profile. A flow rate balance was used to iterate on the total pressure recovery and the capture area to size the inlet.

SUPIN created surface grids of the inlets for visualization. SUPIN also generated three-dimensional, multi-block, structured grids for use with CFD methods.

Wind-US CFD Code

The CFD simulations were performed using the Wind-US CFD code, which solved the Reynolds-Averaged Navier-Stokes (RANS) equations for a multi-block, structured grid for a flow domain about and within the inlet.[4] Figure 4 shows an example of the flow domain used for the streamline-traced inlets. The flow domain had inflow boundaries upstream and about the inlet where freestream boundary conditions were imposed. At the end of the cowl exterior, the domain had an outflow boundary where supersonic extrapolation boundary conditions were imposed. The internal and external surfaces of the inlet formed a portion of the boundary of the flow domain where adiabatic, no-slip viscous wall boundary conditions were imposed. Downstream of the engine face, a converging-diverging nozzle was added to the flow domain to set the flow rate through the inlet. The nozzle throat was set to be choked so that the outflow boundary of the nozzle was supersonic, which allowed non-reflective extrapolation boundary conditions to be imposed.

Wind-US solved the RANS equations in a time-dependent manner for turbulent, compressible flows using a cell-vertex, finite-volume, time-marching approach. A calorically-perfect gas model was used. Turbulence was modeled using the two-equation Menter shear-stress transport (SST) model. Spatial accuracy was formally second-order using the Roe flux-difference splitting upwind formulation. Steady flows were simulated through an iterative process using a first-order,

implicit Euler method with local time-stepping. The flowfield solution was initialized at all grid points with the freestream flow conditions. Iterative convergence of each solution was evaluated through monitoring convergence of the inlet flow rate, total pressure recovery and distortion, and cowl wave drag. The steady-state solution was considered converged when these values varied less than 0.1% of their values over hundreds of iterations. The solution residuals were also monitored to check that they reduced and approached steady values.

Grid convergence was examined by computing the flow solution on a series of grids with varying grid resolutions. Wind-US solved the flow on a sequenced grid in which every other grid point was used. A later section will discuss the grid convergence study that involved four levels of grid resolution.
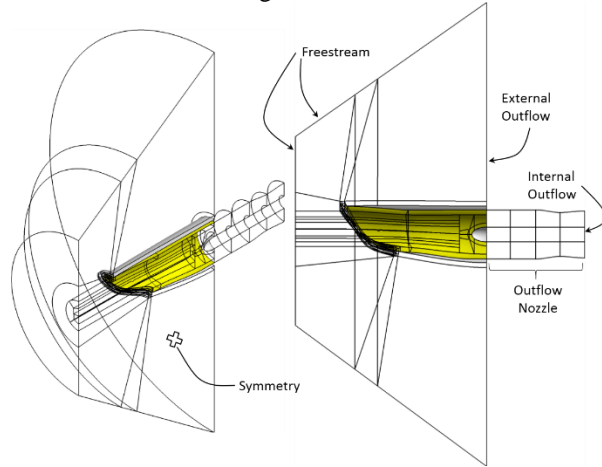
Figure 4. Flow domain and boundary conditions for the CFD analyses.

Porous bleed was modeled as a boundary condition in which the bleed rate was allowed to vary according to local flow conditions.[7] The bleed boundary condition assumed the bleed flow entered a plenum and then was ejected into the freestream through a choked nozzle with a fixed throat area. However, Wind-US does not simulate the bleed exit flow. The primary inputs for the porous bleed model were the porosity of the bleed region and the area of the bleed exit nozzle.

Results

The following sections discuss the inlet designs and results for the aerodynamic performance of the various inlet configurations.

Inlet Design Conditions

The inlets were designed using the same conditions of Ref. 1 which were $M_L = 1.6$ with conditions at an altitude of 40,000 feet. The engine face had a diameter of $D_2 = 3.0$ feet and a spinner hub-to-tip ratio of 0.3. The

engine corrected flow rate was specified with a mass-averaged Mach number of 0.52.

Parent Flowfield Design Factors

The design factors for the parent flowfield were the leading edge angle (θ_{stle}) and the outflow Mach number (M_{stex}). SUPIN was used to explore the effect of varying these factors and Table 1 shows the variation of the length of the supersonic diffuser (L_{EXD}/D_2), Mach number ahead of the terminal shock (M_{EX}), and the total pressure recovery (p_{t2}/p_{t0}). The main effect of θ_{stle} was on the length of the supersonic diffuser. The main effect of M_{stex} was on M_{EX}. The choice of $M_{stex} = 0.90$ showed a slight benefit in the total pressure recovery over $M_{stex} = 0.85$. A primary criteria for the inlet design was to keep $M_{EX} < 1.3$, which reduced the likelihood of boundary layer separation at the interaction of the terminal shock with the boundary layer at the end of the supersonic diffuser. For the current inlet designs, it was decided to use $\theta_{stle} = -5.0$ for a shorter diffuser and $M_{stex} = 0.90$ to keep M_{EX} well below Mach 1.3. For these conditions, the angle of the leading edge shock of the parent flowfield was 135.89 degrees with respect to the positive x-axis. The angle of the terminal shock was $\beta_{stex} = 69.84$ degrees. The angle of the flow at the end of the supersonic diffuser was -4.775 degrees.

Table 1. Results from SUPIN for the variation of the parent flowfield design factors.

θ_{stle} (deg)	M_{stex}	L_{EXD}/D_2	M_{EX}	p_{t2}/p_{t0}
-5.0	0.85	1.039	1.273	0.960
-5.0	0.90	1.041	1.240	0.963
-4.0	0.85	1.083	1.274	0.960
-4.0	0.90	1.085	1.241	0.964

Subsonic Diffuser Design

The subsonic diffuser design involved modification of the shoulder, construction of the subsonic cowl lip, shaping of the subsonic diffuser, and the vertical placement of the engine face.

The shoulder of the inlet was displaced radially outward 0.01 feet to account for boundary layer displacement. The shoulder was then fitted with a circular arc extending over the last 5% of the length of the supersonic diffuser. This provided a smooth surface over which the supersonic diffuser flow turned to the axial direction downstream of the terminal shock.

The subsonic cowl lip was specified to extend over a 120 degree circumference at the bottom of the inlet. The thickness of the subsonic cowl lip at the inlet symmetry plane was specified to be $b_{stcl} = 0.004$ feet. The thickness of the supersonic leading edge was specified to be 0.0004 feet. The leading edge was fitted with an elliptical profile with an aspect ratio of four. The design study considered four levels of the subsonic cowl lip displacement and included $\Delta x_{stcl} = 0.0, 0.12, 0.15,$ and

0.18. These values were normalized by the diameter of the engine face (D_2). The design study considered four levels of the angle of the subsonic cowl lip and included θ_{stcl} = 0, 5, 10, and 15 degrees. Figure 3 showed the effect of these factors and levels on the inlet geometry.

The subsonic diffuser was specified to have a length of 5.04 feet, which matched the length of the STEX-Circular inlet of Ref. 1. This resulted in a length / diameter ratio of 1.68 and an area ratio of 1.28.

The design study considered two levels of the vertical placement of the engine axis, which were y_2 = 1.05 feet and $y_2 = y_{inlet}$ = 1.261 feet. The former value of y_2 moved the engine face downward with respect inlet axis so as to reduce the turning of the surface at the top of the subsonic diffuser.

Baseline Inlet Performance

A baseline inlet configuration was created with the design factors (Δx_{stcl}, θ_{stcl}, y_2) = (0.15, 10, 1.05). Figure 5 shows Mach number contours from the CFD solutions on the symmetry plane of the inlet for (a) subcritical, (b) critical, and (c) supercritical inlet conditions. The white dashed lines show the approximate location of the terminal shock of the parent flowfield. The images show the leading-edge shock and Mach waves along the supersonic diffuser, which approach an intersection point ahead of the subsonic cowl lip.

The displacement of the subsonic cowl lip led to supersonic spillage, which distorted the Mach waves as they approached the subsonic cowl lip region at the bottom of the inlet. For the subcritical condition, the terminal shock was pushed forward to allow subsonic spillage and aligned itself with a local Mach wave. As the terminal shock was pushed forward, the local Mach number ahead of the shock was increased above the Mach 1.24 design condition. This caused the interaction of the terminal shock with the supersonic diffuser boundary layer to be more severe with stronger pressure gradients; however, no boundary layer separation was observed upstream of the shoulder.

The aerodynamic performance of the inlet was measured in terms of the inlet flow ratio (W_2/W_{cap}), mass-averaged total pressure recovery at the engine face (p_{t2}/p_{t0}), total pressure distortion descriptors (*DIST, IDR, IDC*), and cowl wave drag (C_{Dwave}). The inlet flow rate (W_2) was obtained from the CFD solution through integration of the flow through grid planes along the axis of the outflow nozzle. The inlet capture flow rate (W_{cap}) was computed from the freestream conditions and the inlet capture area. The cowl wave drag coefficient was computed through integration of the static pressures on the cowl exterior. The inlet capture area was used as the reference area.

Figure 6 shows the characteristic curve for the baseline inlet. The "a", "b", and "c" labels correspond to the subcritical, critical, and supercritical conditions

and labels of Fig. 5. Also plotted are the characteristic curves from Ref. 1 for the axisymmetric spike and STEX-Circular inlets. The dashed line of Fig. 6 represents the expected recovery for an inlet at Mach 1.6 according to MIL-E-5007D. The baseline inlet reduced the spillage and increased the total pressure recovery with respect to the STEX-Circular inlet.
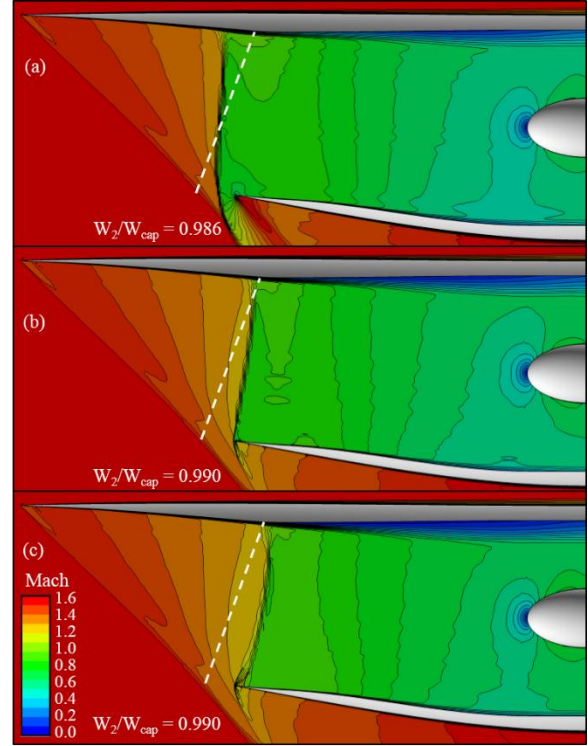

Figure 5. Mach number contours on the symmetry plane for the baseline inlet.
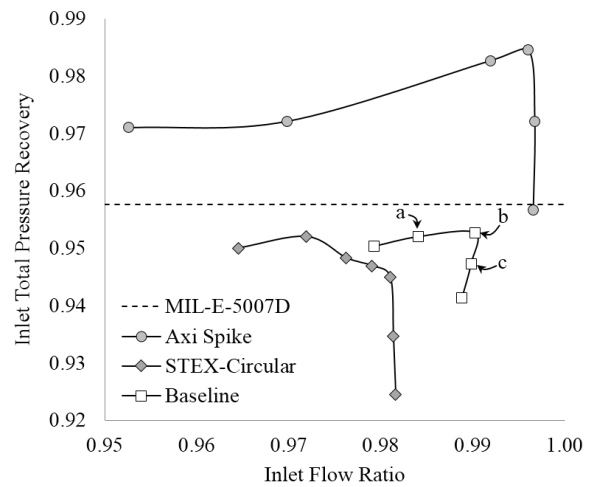

Figure 6. Characteristic curves for the baseline, axisymmetric spike, and STEX-Circular inlets.

Figure 7 shows the total pressure and Mach number contours at the engine face from the Wind-US solution at the critical inlet condition. The total pressures were normalized by the freestream total pressure. The total pressure contours show a combination of radial and circumferential distortion due to thicker boundary layers at the top of the subsonic diffuser. The boundary layer developed along the length of the supersonic diffuser and then was thickened due to the interaction with the terminal shock. Further, the boundary layer was turned past the shoulder. All of these presented difficult conditions for the boundary layer. The scarfed nature of the supersonic diffuser results in a slight circumferential distortion. The spinner accelerates the core inlet flow toward Mach 0.7 at the engine face.
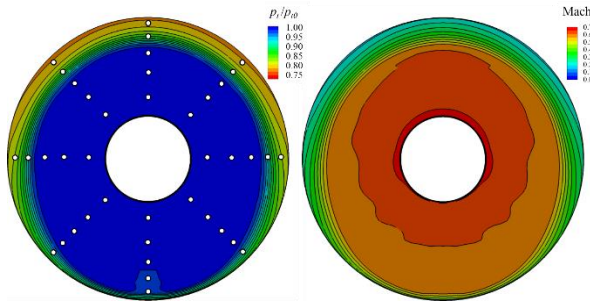
Figure 7. Total pressure recovery and Mach number contours at the engine face for point (b) of the baseline inlet flowfield.

The white circles on the contour plot of the total pressures of Fig. 7 indicate the location of probes of an equal-area 40-probe rake created using SAE 1420 recommendations.[8] The CFD solution was interpolated onto the probe locations and the total pressures were used to determine total pressure distortion descriptors. The descriptors included a simple *DIST* descriptor which was the difference of the maximum and minimum probe total pressures normalized by the average total pressure of all of the probes. Two other distortion descriptors were the General Electric radial tip (*IDR*) and circumferential (*IDC*) descriptors.[9]

For the total pressure of the rake of Fig. 7, the values of the distortion descriptors were *DIST* = 0.1952, *IDR* = 0.0918, and *IDC* = 0.0591. The impact of these distortion descriptors depends on the distortion limits of the respective engine of interest. Reference 10 lists distortion limits for the F404-GE-400 engine which are *IDR* < 0.10 and *IDC* < 0.20. Based on these limits, the baseline inlet at the critical conditions has acceptable distortion levels.

Grid Convergence Study

A series of CFD simulations were performed for the baseline inlet to evaluate the convergence of the total pressure recovery, distortion, flow rates, and cowl drag with respect to the resolution of the computational grid.

The primary factors for grid resolution were the axial spacing within the throat of the inlet (Δs_{thrt}) and the circumferential grid spacing (Δs_{sym}). Two computational grids were generated with (Δs_{thrt}, Δs_{sym}) = (0.013, 0.020) and (0.018, 0.024), respectively. The values of the grid spacing were normalized by the diameter of the engine face. Both grids used a wall normal grid spacing of 3.0×10^{-5} feet, which resulted in a normalized wall coordinate of $y^+ \approx 2.0$ throughout most of the inlet. Both grids consisted of 29 structured blocks. The coarser grid contained a total of 2.634×10^6 grid points while the finer grid contained 4.215×10^6 grid points. Within the internal ducting of the inlet, the number of axial grid points for the coarser and finer grids were 209 and 284 grid points, respectively. The coarser and finer grids contained 65 and 81 circumferential grid points, respectively. On the symmetry plane, the coarser and finer grids contained 201 and 260 grid points, respectively, between the bottom of the interior surface of the inlet to the top of the interior surface. The Wind-US CFD code sequenced the grids to solve the flow on a coarser grid consisting of every other grid point. Thus, with the sequencing of each of the coarser and finer grids, flow solutions were computed on four levels of grid resolution. Table 2 lists the results of the grid convergence study. The reference grid spacing (Δs^*_{ref}) was computed as the root-mean-square of Δs_{thrt} and Δs_{sym} normalized by the value of the root-mean-square for the finest grid. Listed are the normalized corrected flow rate (W_{C2}/W^*_{C2}), total pressure recovery (p_{t2}/p_{t0}), cowl wave drag (C_{Dwave}), and distortion index (*DIST*) for solutions close to the critical condition of the inlet on each of the four grid levels. All of the simulations had the same outflow nozzle throat radius. The values showed very little variation. The value Δ_{max} was the maximum absolute difference between the highest and lowest values normalized by the value for the finest grid. Most values were about 0.2%. The results indicated that the coarser grid was sufficient to provide grid convergence, and so, was used for the CFD simulations.

Table 2. Grid convergence study results.

Δs^*_{ref}	W_{C2}/W^*_{C2}	p_{t2}/p_{t0}	C_{Dwave}	*DIST*
2.55	1.0157	0.9510	0.0393	0.1941
2.00	1.0153	0.9514	0.0400	0.2000
1.27	1.0138	0.9527	0.0408	0.1952
1.00	1.0137	0.9528	0.0409	0.1943
Δ_{max}	0.21%	0.19%	0.16%	0.62%
SUPIN	1.0000	0.9756	0.0271	-
$\Delta\%$	1.37%	-2.39%	-33.7%	-

Also listed in Table 2 are the values of the total pressure recovery and wave drag as computed by SUPIN. This provided a check on how closely SUPIN agreed with the Wind-US. SUPIN was optimistic in estimating the total pressure recovery, which was likely

due to the lack of models within SUPIN to compute total pressure losses for the shock wave / boundary layer interaction and increased boundary layer growth in the subsonic diffuser. SUPIN computed much lower cowl wave drag. The reasons for this are not fully understood at this time.

Effect of the Subsonic Cowl Lip Displacement

The amount of subsonic cowl lip displacement is set by the Δx_{stcl}, which is normalized by the diameter of the engine face. Figure 8 shows Mach number contours on the symmetry plane from Wind-US solutions of four inlets with varying levels of displacement. The top image is for an inlet with zero displacement ($\Delta x_{stcl} = 0.0$). As in Fig. 5, the leading edge shock and Mach waves of the supersonic diffuser can be seen. For zero displacement, the shock and Mach waves are directed to intersect with the subsonic cowl lip and there is essentially no supersonic spillage. The white dashed line indicates the design location and angle of the terminal shock of the parent flowfield. The terminal shock of the CFD solution is shown downstream of the design location and represents the closest solution to critical operation for this inlet. When the corrected engine flow was decreased by just 0.78%, the terminal shock was pushed upstream of the subsonic cowl lip, as shown by the top image of Fig. 9. Such behavior is similar to an unstart behavior of a mixed-compression inlet.

Figure 8 shows the images for the three other inlets with varying subsonic cowl lip displacement for solutions near critical operation. Figure 9 shows similar images for the same inlets at subcritical operation. Figures 8 and 9 show that with increased subsonic cowl lip displacement, the terminal shock involved less forward motion as the inlet operation changed from critical to subcritical. Another way of looking at this is shown in Fig. 10 with the plots of the characteristic curves and corrected engine flow curves for the four inlets. For the characteristic curves, as the level of subsonic cowl lip displacement was increased, the subcritical legs of the curves became less steep, which indicates less rate of decrease of the total pressure recovery with decreased engine flow ratio. This is consistent with less forward travel of the terminal shock into higher Mach number flows of the supersonic diffuser. This also can be observed as "flatter" corrected flow curves with increased displacement, as shown in the bottom plots of Fig. 10. The curves of Fig. 10 for the inlet with zero subsonic cowl lip displacement exhibited a hysteresis phenomenon not observed for the inlets with displacement. When the inlet solutions were computed from supercritical solutions, the solid line was generated. The large jump from point 3 to point 2 represents the "unstart" behavior mentioned above and shown as the top images of Figs. 9 and 10, respectively. The dashed line of Fig. 10 show the solutions obtained from

initializations using subcritical solutions. The first four points of the curve remain as subcritical operation. At the corrected flow rate of the fifth point, the inlet swallows the shock or "self-starts" and the supercritical solution is obtained.
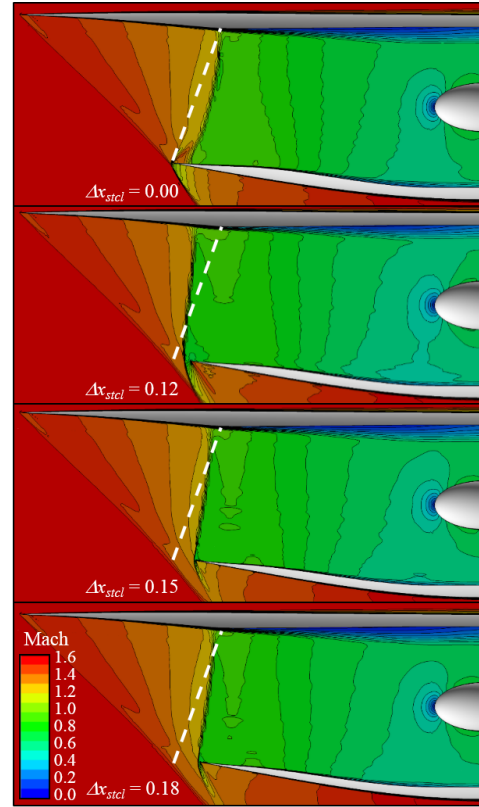

Figure 8. Mach number contours on the symmetry plane for critical operation for the four levels of subsonic cowl lip displacement.

It became apparent that subsonic cowl lip displacement was needed for good inlet operation. A choice of $\Delta x_{stcl} = 0.15$ represented the best choice for these inlet conditions to maximize the total pressure recovery and reduce spillage, while still allowing spillage to provide stable shock behavior.

Another feature of the flow became apparent in Fig. 9 during subcritical operation. The image at the top of Fig. 9 for the inlet with zero displacement shows circumferential distortion for the bottom third of the engine face. Vortices can be seen at the 75 and 225 degree locations. These vortices originate from the interaction of the subcritical terminal shock with the edges of the subsonic cowl lip. Small levels of distortion showed up for the inlet with $\Delta x_{stcl} = 0.12$, but are not seen for the inlets with greater subsonic cowl lip displacement. This suggests that the subsonic cowl lip displacement reduces this type of distortion by allowing subsonic spillage with less forward motion of the subcritical terminal shock.
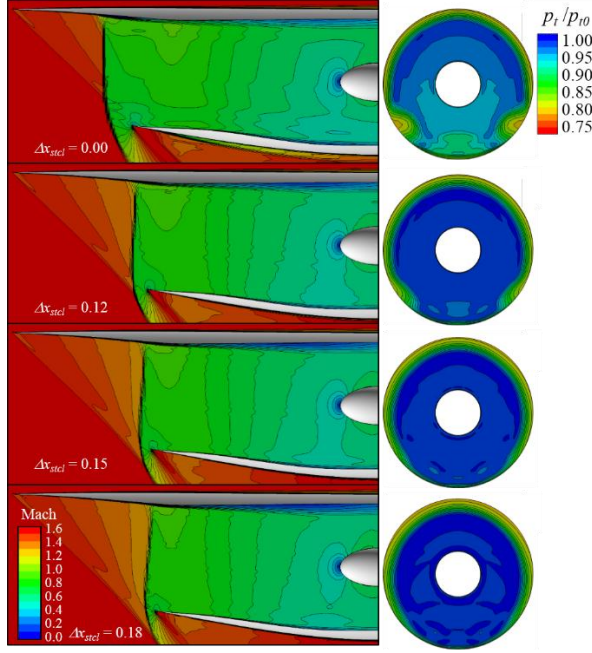
Figure 9. Mach number contours on the symmetry plane and total pressures at the engine face for subcritical operation for the four levels of subsonic cowl lip displacement.
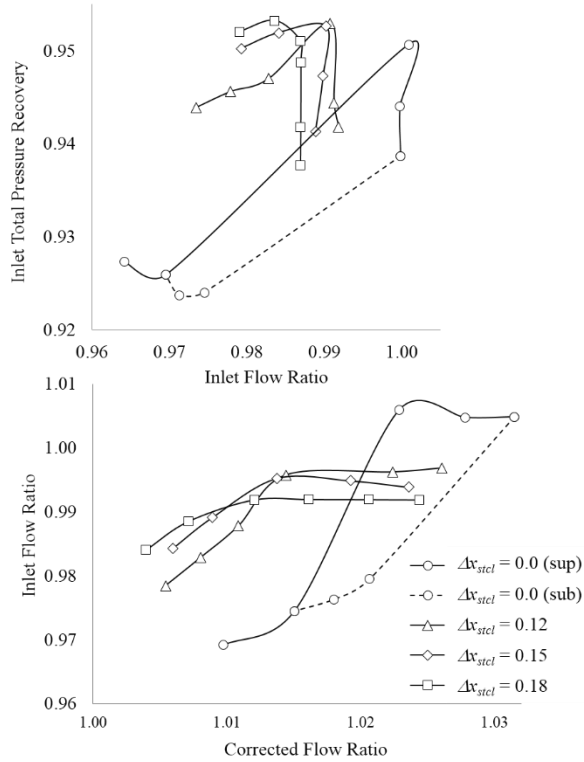

Figure 10. Characteristic and corrected flow curves for the four levels of subsonic cowl lip displacement.

Effect of the Subsonic Cowl Lip Angle

The angle of the subsonic cowl lip at the inlet symmetry plane (θ_{stcl}) was varied to explore its effect. Figure 11 shows Mach number contours and momentum velocity vectors in the vicinity of the subsonic cowl lip on the symmetry plane. Shown in the image is the terminal shock at the left of the image and subsonic flow downstream of the terminal shock. The momentum vectors show the local flow angle downstream of the terminal shock. These angles vary between -10 and -15 degrees with respect to the positive *x*-axis. The outline of the subsonic cowl lip is shown with $\theta_{stcl} = -15$ degrees, which is approximately lined up with the local flow direction.
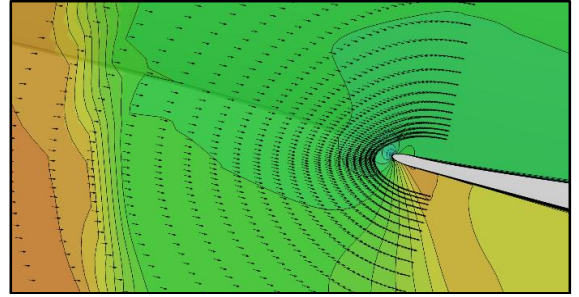
Figure 11. Mach contours and momentum vectors on the symmetry plane showing alignment of the subsonic cowl lip with the local flow direction.

Figure 12 shows the characteristic curves for the four inlets. The greatest effect of increased subsonic cowl lip angle seemed to be to move the critical point to the right and upward. The critical point of the curve becomes more defined and sharper with increased angle.
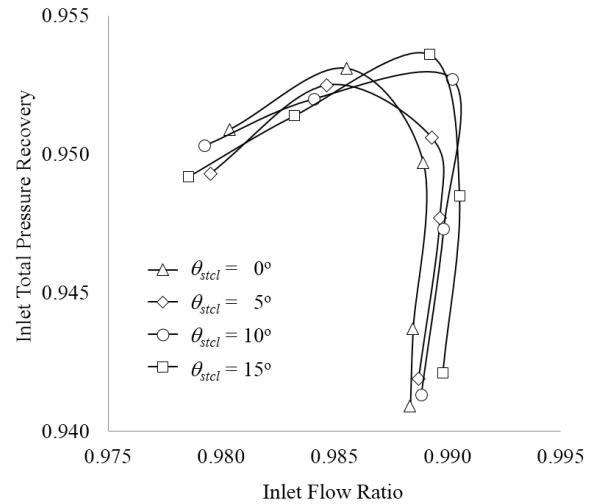

Figure 12. Characteristic curves for the variation in the subsonic cowl lip angle.

Table 3 lists the results for the inlet performance at the critical operation of each of the inlets. The wave drag shows a slight increase as the subsonic cowl lip angle is increased. The distortion descriptor is reduced with increased angle.

Table 3. Results for the variation of the angle of the subsonic cowl lip.

θ_{stcl} (deg)	$W_{C2}/W_{C2}{}^*$	p_{t2}/p_{t0}	C_{Dwave}	DIST
0.0	1.0158	0.9497	0.0404	0.2191
5.0	1.0152	0.9506	0.0401	0.2092
10.0	1.0138	0.9527	0.0408	0.1952
15.0	1.0124	0.9536	0.0429	0.1787

Best Inlet Configuration

A "best" inlet configuration was considered to be the inlet with the subsonic cowl lip angle of $\theta_{stcl} = 15$ degrees and subsonic cowl lip displacement of $\Delta x_{stcl} = 0.15$. Figure 13 shows the characteristic curve for the best configuration compared to the baseline. There was only a slight improvement over the baseline because the only difference between the configurations is 5 degrees of the subsonic cowl lip angle.
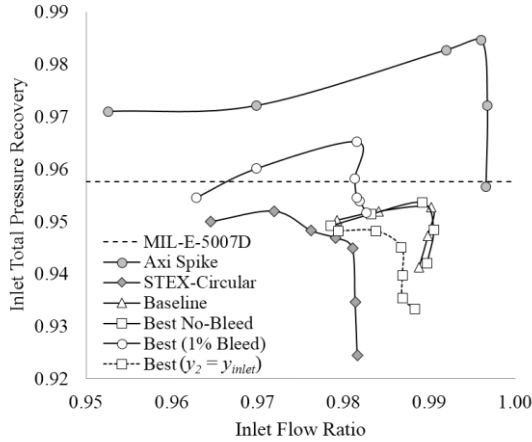
Figure 13. Characteristic curves for the "best" inlet without bleed, with 1% bleed, and with y_2 set equal to y_{inlet}.

Figure 14 shows the *IDR* and *IDC* distortion descriptors for the inlets. Also plotted in Fig. 14 are the limits on IDR and IDC, as obtained from Ref. 10. For IDC < 0.05, the limit on IDR is reduced, such that, when there is no circumferential distortion, the limit on the radial distortion is IDR < 0.05. This behavior on the limit for IDR was due to instances of flutter of the F404 fan blades during aeromechanical testing with radial distortion patterns. The "best" inlet does reduce circumferential distortion compared to the STEX-Circular inlet; however, the radial distortion is greater. The axisymmetric character of the Axi-Spike inlet simulations resulted in essentially no circumferential distortion.

Effect of Porous Bleed

The "best" inlet configuration was then resized to allow for 1% porous bleed in the subsonic diffuser. The bleed region was positioned downstream of the shoulder to assist in reducing the growth of the boundary layer. Figure 15 shows contours of Mach number on the symmetry plane for the "best" inlet configurations with and without bleed for CFD solutions near critical operation. The middle image shows the region over which the porous bleed boundary conditions were applied. Figure 16 shows the total pressures at the engine face for the three cases. The effect of bleed is to reduce the size and extent of the low-momentum region at the top of the subsonic diffuser and engine face. The characteristic curves of Fig. 13 show that the bleed improves the total pressure recovery above the MIL-E-5007D level. Figure 14 shows that the radial and circumferential distortion levels decreased with respect to the "best" no-bleed inlet and fall within the limits.
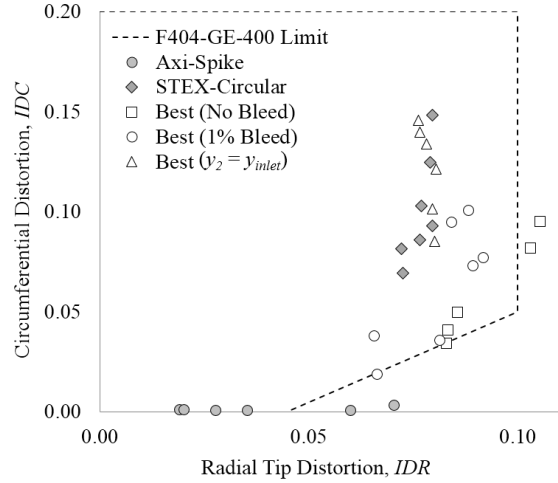

Figure 14. Distortion descriptors for the "best" inlet configurations.

Effect of Engine Axis Placement

The "best" inlet configuration was modified to place the engine axis collinear with the inlet axis ($y_2 = y_{inlet}$) to explore its effect. This introduced greater turning at the top of the subsonic diffuser, which resulted in a larger low-momentum region. Figure 13 shows the reduction of total pressure recovery. Curiously, Fig. 14 shows that while the circumferential distortion was greater than for the "best" inlet, the distortion was within the limits. The distortion was also similar to that of the STEX-Circular inlet, which also had $y_2 = y_{inlet}$. While displacement of the engine axis downward is beneficial, the position of the engine with respect to the inlet for an actual inlet-aircraft integration may be specified as part of the design problem rather allowed to be an inlet design factor.
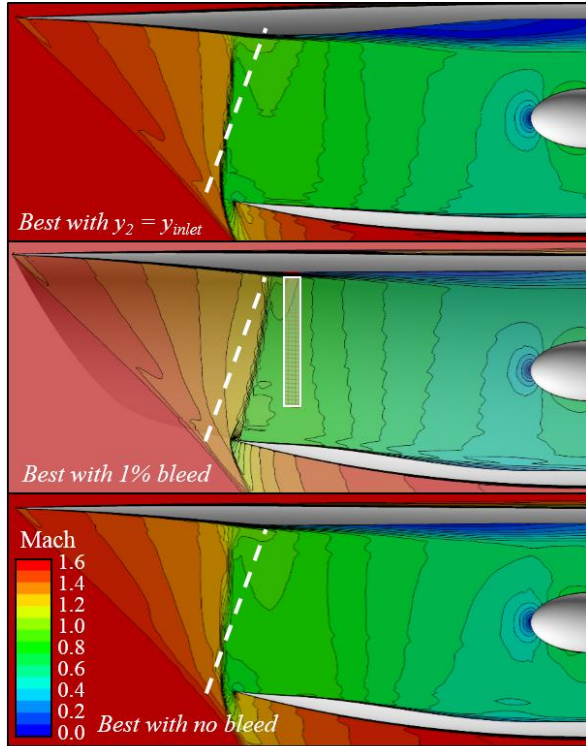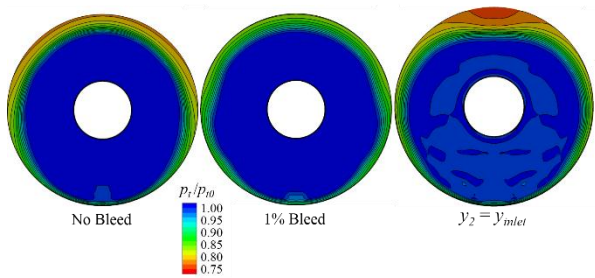
Figure 15. Mach number contours for the "best" inlets.

Figure 16. Total pressure contours at the engine face for the "best" inlet configurations.

Conclusions

The aerodynamic performance of the streamline-traced inlets was enhanced through use of an improved parent flowfield, judicious engine axis placement, best subsonic cowl lip factors, and porous bleed. The results of the CFD simulations and factor variations provided information that allowed a greater understanding of the aerodynamic performance of streamline-traced external-compression inlets for Mach 1.6. Future efforts will study the effect of vortex generators to mix the flow to reduce the low-momentum region at the top of the subsonic diffuser and engine face. The streamline-traced inlets will also be analyzed for off-design conditions of lower supersonic and subsonic Mach numbers, angle-of-attack, and angle-of-sideslip.

References

[1] Slater, J. W., "Methodology for the Design of Streamline-Traced, External-Compression Inlets," AIAA-2014-3593, July 2014.

[2] Otto, S. E, Trefny, C. J., and Slater, J. W., "Inward-Turning Streamline-Traced Inlet Design Method for Low-Boom, Low-Drag Applications," AIAA-2015-3593, July 2015.

[3] Slater, J. W., "Design and Analysis Tool for External-Compression Supersonic Inlets," AIAA-2012-0016, January 2012.

[4] Mani, M., Cary, A., and Ramakrishnan, S., "A Structured and Hybrid-unstructured Grid Euler and Navier-Stokes Solver for General Geometry," AIAA-2004-0524, January 2004.

[5] Mölder, S., "Internal, Axisymmetric, Conical Flow," *AIAA Journal*, Vol. 5, No. 7, 1967, pp. 1252-1255.

[6] Anderson, J.D., Jr., *Modern Compressible Flow*, McGraw-Hill Book Company, New York, 1982.

[7] Slater, J. W., "Improvement in Modeling 90-degree Bleed Holes for Supersonic Inlets," *AIAA Journal of Propulsion and Power*, Vol. 28, No. 4, 2012, pp 773-781.

[8] Society of Automotive Engineers (SAE), "Gas Turbine Engine Inlet Flow Distortion Guidelines," SAE ARP 1420, Rev. B, February 2002.

[9] Moore, M. T. "Distortion Data Analysis", Report AFATPL-TR-72-111, February 1973.

[10] Steenken, W. G., Williams, J. G., Yuhas, A. J., and Walsh, K. R., "An Inlet Distortion Assessment during Aircraft Departures at High Angle of Attack for an F/A-18A Aircraft," NASA TM-104328, 1997.